Optically Detected Magnetic Resonance in Neutral Silicon Vacancy Centers in Diamond via Bound Exciton States

Zi-Huai Zhang,[1] Paul Stevenson,[1] Gergő Thiering,[2,3] Brendon C. Rose,[1] Ding Huang,[1] Andrew M. Edmonds,[4] Matthew L. Markham,[4] Stephen A. Lyon,[1] Adam Gali,[2,3] and Nathalie P. de Leon[1,*]

[1]*Department of Electrical Engineering, Princeton University, Princeton, New Jersey 08544, USA*
[2]*Wigner Research Centre for Physics, P.O. Box 49, H-1525 Budapest, Hungary*
[3]*Department of Atomic Physics, Budapest University of Technology and Economics, Budafoki út 8., H-1111 Budapest, Hungary*
[4]*Element Six, Harwell OX11 0QR, United Kingdom*

(Received 30 April 2020; accepted 22 October 2020; published 30 November 2020)

Neutral silicon vacancy (SiV^0) centers in diamond are promising candidates for quantum networks because of their excellent optical properties and long spin coherence times. However, spin-dependent fluorescence in such defects has been elusive due to poor understanding of the excited state fine structure and limited off-resonant spin polarization. Here we report the realization of optically detected magnetic resonance and coherent control of SiV^0 centers at cryogenic temperatures, enabled by efficient optical spin polarization via previously unreported higher-lying excited states. We assign these states as bound exciton states using group theory and density functional theory. These bound exciton states enable new control schemes for SiV^0 as well as other emerging defect systems.

DOI: 10.1103/PhysRevLett.125.237402

Point defects in solid-state materials are promising candidates for quantum memories in a quantum network. These quantum defects combine the excellent optical and spin properties of isolated atoms with the scalability of solid-state systems [1–3]. Long-range, kilometer-scale entanglement generation has been demonstrated with the nitrogen vacancy (NV) center in diamond [4]. However, the entanglement generation rate in such demonstrations is limited by the optical properties of the NV center, which exhibits significant spectral diffusion [5,6] and a small Debye-Waller factor [7]. The neutral silicon vacancy center in diamond (SiV^0) has the potential to mitigate many of these problems; its inversion symmetry guarantees a vanishing permanent dipole moment, which minimizes spectral diffusion, and over 90% of its emission is in the zero-phonon line (ZPL) [8]. However, there has been no report of optically detected magnetic resonance (ODMR) for this defect, a key first step towards establishing a spin-photon interface, and the electronic structure of SiV^0 is still not well understood [9]. A detailed understanding of the optical transition and excited state structure of SiV^0 is key in developing preparation, manipulation and readout schemes for quantum information processing applications.

In this work, we present the observation of previously unreported optical transitions in SiV^0 that are capable of efficiently polarizing the ground state spin. Previous studies on SiV^0 have reported a strong ZPL transition at 946 nm, and a weaker strain-activated transition at 951 nm [9]. Through a combination of optical and electron spin resonance (ESR) measurements, we are able to assign groups of transitions from 825 to 890 nm to higher-lying excited states of SiV^0. We interpret these spectroscopic lines as transitions to bound exciton (BE) states of the defect. We observe highly efficient bulk spin polarization through optical excitation of these transitions, providing another manifold of states that can be used for spin initialization. Spin polarization via these BE states while collecting emission from the ZPL and phonon sideband enables the observation of ODMR. We use ODMR measurements to probe the low magnetic field behavior of SiV^0 where we observe no spin relaxation (T_1) out to 30 ms, spin dephasing times (T_2^*) of 202 ns, and spin coherence times (T_2) of 55.5 μs at 6 K.

We observe ODMR in an ensemble of SiV^0 centers using excitation at one of the BE transitions (855.65 nm) in a chemical-vapor deposition grown sample doped with isotopically enriched ^{29}Si during growth, described previously in Ref. [10]. As the microwave frequency is swept across the zero-field splitting of SiV^0, we observe three resonance peaks in continuous-wave (CW) ODMR [Fig. 1(a)]. The two outer peaks correspond to spin transitions associated with centers containing ^{29}Si, while the central peak at 944 MHz is associated with ^{28}Si and ^{30}Si. The position and splitting of the lines are consistent with previously measured hyperfine parameters [11].

We realize coherent control using pulsed ODMR on the lower frequency ^{29}Si hyperfine transition at 912 MHz and observe Rabi oscillations that decay over 499 ± 28 ns [Fig. 1(b)]. We measure the spin dephasing time to be $T_2^* = 202 \pm 16$ ns [Fig. 1(c)] using a Ramsey sequence.

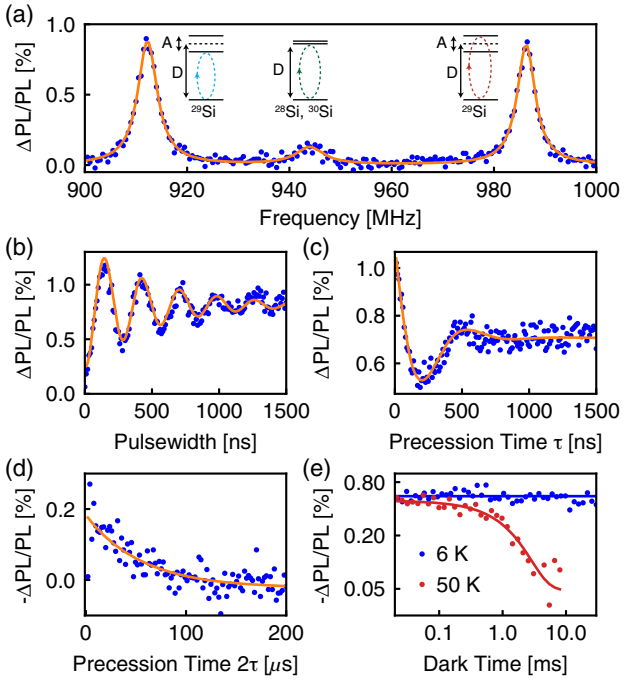

FIG. 1. Optically detected magnetic resonance and coherent properties of SiV^0 spins. (a) CW ODMR spectrum measured at 6 K. The two outer peaks correspond to two hyperfine lines associated with the ^{29}Si nucleus and the central peak is associated with ^{28}Si and ^{30}Si species. The solid line is a Lorentzian fit and the linewidths are microwave power broadened. Inset: relevant energy levels for individual spin transitions, where D denotes the zero-field splitting and A denotes the hyperfine interaction from the ^{29}Si nucleus. (b) Rabi oscillation measured at 6 K performed at the lower hyperfine transition at 912 MHz. The data is fitted using $a \times e^{-t/T} \cos(\omega t + b) + c$ with $T = 499 \pm 28$ ns. (c) Spin dephasing time (T_2^*) measured at 6 K using a Ramsey sequence with microwave frequency detuned from the spin resonance by 1.6 MHz. The decay is fitted using $a \times e^{-\tau/T_2^*} \cos(\omega\tau + b) + c$ with $T_2^* = 202 \pm 16$ ns. (d) Spin coherence time (T_2) measured at 6 K with a Hahn echo sequence. The decay is fitted using $a \times e^{-2\tau/T_2} + b$ with $T_2 = 55.5 \pm 10.6$ μs. The relatively large fitting error is due to the partially resolved modulation (see Supplemental Material Sec. III A [12]). (e) Spin relaxation times (T_1) measured at 6 K and 50 K. At 6 K, no decay is observed up to 30 ms. The blue line is a flat line as a guide to the eye. At 50 K, we observe an exponential decay with a decay constant 1.38 ± 0.21 ms. The red line is a fit to the data with the form $a \times e^{-t/T_1} + b$. ODMR measurements are performed at ambient magnetic field.

By using a Hahn echo sequence to refocus the coherence, we measure the spin coherence time to be $T_2 = 55.5 \pm 10.6$ μs [Fig. 1(d)]. The spin coherence time measured here is shorter than previous measurements of this sample using X-band pulsed ESR, $T_2 = 280$–480 μs [10]. This likely arises from the high density of SiV^0 centers in this sample, which gives rise to instantaneous diffusion [10,38]. At ambient magnetic fields, the effects of instantaneous diffusion are more pronounced because centers of different orientations and nuclear spin projections are nearly degenerate. This effect limits T_2 to 56 μs (see Supplemental Material Sec. III B [12]).

We measure the spin relaxation time (T_1) using pulsed ODMR by measuring spin population decay after a variable dark time between the initialization and readout pulses. We observe no decay up to 30 ms at 6 K [Fig. 1(e)], consistent with previous measurements of $T_1 = 46$ s at this temperature [10]. At higher temperatures, the spin lifetime shortens significantly due to an Orbach process with an activation energy of 16.8 meV [10] and we measure $T_1 = 1.38 \pm 0.21$ ms at 50 K.

Our temperature-dependent ODMR T_1 measurements on the lower hyperfine transition are consistent with the previously measured activation energy (see Fig. S7 [12]), but we observe the Orbach rate prefactor to be ~260 times larger. This is largely due to hyperfine-induced mixing of the SiV^0 spin states (see Supplemental Material Sec. III C [12]). The hyperfine interaction for SiV^0 is ~30 times larger than that for the NV center and the zero-field splitting is three times smaller [11,39], so at low magnetic field the influence of the hyperfine interaction is much more pronounced. Unlike nitrogen, however, silicon has spin-free nuclear isotopes which may be used to circumvent these effects.

The observation of ODMR in SiV^0 is enabled by the discovery of additional higher-lying excited states beyond the ZPL. Previous studies on SiV^0 excited states were limited to the ^3E_u (ZPL at 946 nm) and $^3A_{2u}$ (ZPL at 951 nm) states but higher energy states were never explored. Transitions between 820 and 950 nm in silicon-doped diamonds have been previously observed with photoconductivity and absorption measurements, but there has been no detailed spectroscopy of these spectral lines, nor assignment of their microscopic origin [40–42].

In order to probe whether these transitions are associated with the SiV^0 center, we correlate several types of optical spectroscopy at low temperature (5.5 K) at ambient magnetic field. First we perform absorption spectroscopy over a large wavelength range, from the ionization threshold (~826 nm [40]) to 900 nm. We observe several families of peaks near 830, 855 and 870 nm [Fig. 2(a)]. Then we perform photoluminescence excitation (PLE) spectroscopy, wherein we excite at these absorption wavelengths and detect emission at 946 nm, the ZPL of SiV^0. We observe the same clusters of resonances in PLE, confirming that the transitions are associated with the SiV^0 center [Fig. 2(b)].

Finally, we probe the interaction between these higher lying transitions and the ground state spin of SiV^0 by measuring optical spin polarization (OSP) in bulk ESR (~3100 G) after excitation at these wavelengths [Fig. 2(c)]. Specifically, we use a pump-probe measurement to isolate the contributions from $m_s = 0$ (I_0) and $m_s = 1$ (I_1) spin states (see Supplemental Material Sec. VI [12]). Remarkably, the bulk OSP reaches values up to 40%–60%

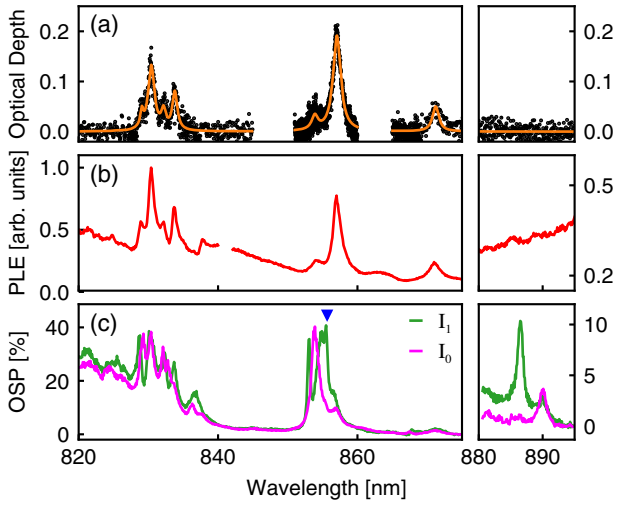

FIG. 2. Spectroscopy and spin polarization of higher-lying excited states. (a) Absorption measurements at 5.5 K showing narrow absorption peaks. The raw data is baseline subtracted to eliminate contribution from broadband absorption. The orange curve shows a Lorentzian fit to the data. (b) PLE measurement at 5.5 K with detection at 946 nm showing resonant features that line up with the observed absorption peaks. (c) Pump-probe OSP measurement at 5.5 K showing narrow resonances after initialization into $m_s = 0$ (I_0, magenta) or $m_s = 1$ (I_1, green). The amplitude of each spectrum I_i represents probe induced population change of sublevel $m_s = i$, with the baseline subtracted. The blue triangle denotes the wavelength used for ODMR measurements. The wavelength range from 875 to 880 nm is not shown.

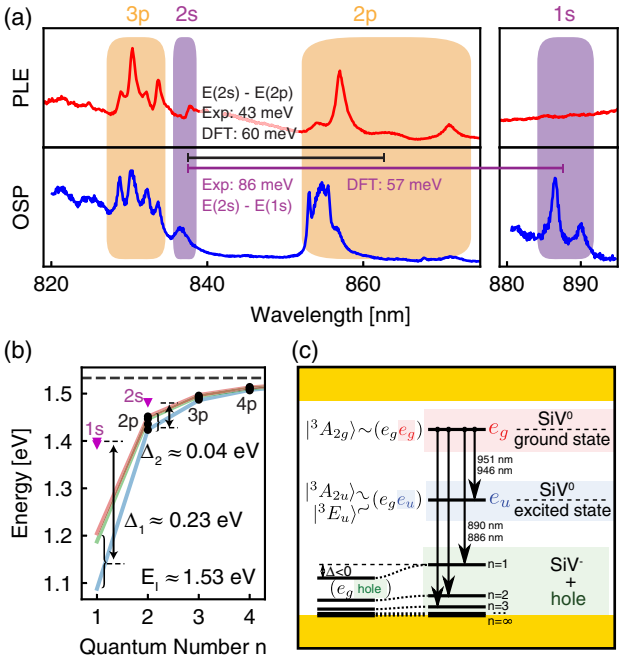

FIG. 3. s- and p-like states in PLE and ESR measurements. (a) State assignments and comparison of experimental and calculated energy splittings. The upper panel shows PLE spectra. The lower panel is constructed using decomposed OSP spectra as $2I_1 + I_0$ to resemble absorption. (b) Scaling of the peak positions extracted from PLE in (a). The fit uses Rydberg scaling $E_n = E_I - E_y/n^2$. Because of similar fine structures of $2p$ and $3p$ states, we fit different fine structure transitions separately corresponding to the different colored curves. The fitted ionization energy (E_I) and Rydberg energy (E_y) are 1.53 and 0.4 eV, respectively. The horizontal dashed line indicates the fitted ionization energy. States with s-like character are taken from spin-polarization measurements, and are shown with triangles. Δ_1 and Δ_2 are energy deviations for $1s$ and $2s$ states compared to the fitted Rydberg scaling that involve both central cell correction and the localized phonon energy. (c) Proposed bound exciton model for the higher-lying excited states showing orbital ground and excited states and BE states at higher energies in the hole picture. The lower levels closer to the valence band maximum for electrons require higher excitation energy.

(see Supplemental Material Sec. V [12]), a key enabling capability for the observation of ODMR.

Using OSP measurements, we also observe a new cluster of transitions near 886 nm that are not evident in absorption or PLE spectroscopy [Fig. 2(c), right]. This indicates that these transitions have a weak oscillator strength, but are strongly spin polarizing.

The number of observed transitions cannot be described by models utilizing only the orbitals localized on the SiV^0 center. Group theoretic considerations describe three triplet excited configurations for SiV^0: ^3E_u, $^3A_{1u}$ and $^3A_{2u}$ [43]. Bulk photoluminescence measurements under uniaxial stress suggest that the 946 nm transition arises from the ^3E_u state and the 951 nm transition arises from the $^3A_{2u}$ state [9]. Only the transition from the $^3A_{1u}$ state has not been experimentally identified.

The proximity of several of these resonances to the ionization threshold of SiV^0 (~826 nm [40]) provides a clue to their nature. We propose that SiV^0 can act as a pseudo-acceptor, forming BE states composed of a hole weakly bound to a transiently generated SiV^- center. BE states of neutral defects have been observed in SiC [44,45], Si [46–50], and GaP [51]. One manifestation of BE states is a progression of peaks that can be described qualitatively as transitions between hydrogenic states and labeled with principal quantum numbers, n, and angular momentum labels (s, p, d, etc.). These progressions are observed in both PLE and OSP measurements, shown in Fig. 3(a). A schematic level diagram for the states described here is depicted in Fig. 3(c). Based on this model, transitions to "s"-like states are expected to be electric-dipole forbidden, since both the ground state and BE state are of *gerade* symmetry. Indeed, we observe transitions at 886 and 837 nm in OSP, but not in absorption or PLE. The isotopic shift of the $1s$ transition suggests that this transition is phonon assisted in nature (see Supplemental Material Sec. VII [12]). We fit the observed energies (E_n) of the "p"-like transitions to the Rydberg scaling, $E_n = E_I - E_y/n^2$, shown in Fig. 3(b), where E_I is the ionization energy and E_y is the Rydberg energy. We find the fitted

ionization energy E_I to be in good agreement with photoconductivity measurements [40], and the Rydberg energy to be consistent with an effective-mass description of the system (see Supplemental Material Sec. VIII A [12]).

The s-like states were excluded from this analysis because of their vibronic nature and the central-cell correction expected for these types of states [52]. This expectation is borne out in density functional theory (DFT) calculations (see Fig. S20 and Supplemental Material Sec. IX G [12]), where the calculated $1s$–$2s$ energy difference of 57 meV is in better agreement with experimental measurements (86 meV) than the > 250 meV difference expected from a hydrogenic model without a central cell correction. The calculated energy difference between the $2s$ and $2p$ states is also consistent with experimental observations [Fig. 3(a)]. The central cell correction arises because the BE states are effectively excluded from occupying the 6 carbon atoms adjacent to the SiV^- center, increasing the effective Bohr radius and decreasing the effective Rydberg energy. This effect is less pronounced for p-like states because they have radial nodes at the SiV^- center.

Within each labeled manifold in Fig. 3(a), significant structure is observed. This likely arises from a combination of spin-orbit structure in the valence band, crystal-field interactions from the presence of the symmetry-lowering SiV^0 defect, and coupling between the bound hole and SiV^-. We note that the bulk inhomogeneous linewidth likely obscures the full multiplicity of these transitions.

Transitions above the $n = 3$ level are not clearly observable in the experimental data. We believe this is a combination of the oscillator strength scaling (n^{-3}), proximity to the ionization threshold, and competition with other nonradiative, non-spin-polarizing relaxation pathways.

With this model for the nature of the transitions, we now turn to the details of the spin polarization and ODMR contrast. The magnitude of the ODMR signal depends sensitively on the excitation wavelength, and we observe resonant features that match the linewidths observed in absorption, PLE, and OSP measurements for the $n = 2$ and $n = 3$ BE transitions [Fig. 4(a), upper panel]. This is in stark contrast to ODMR in the NV center, which shows significant ODMR contrast for off-resonant excitation due to its spin dependent intersystem crossing. This indicates that the mechanism for ODMR relies on selective excitation of these transitions, which can arise from both the resonant nature of OSP and spin-selective optical pumping leading to population shelving into a "dark" spin state.

Furthermore, we observe that the ODMR signal can be both positive and negative. Optical transitions with nonunity cyclicity lead to population of ground states (e.g., other m_s levels here) that are not addressed by the spectrally narrow excitation [Fig. 4(b)]. This process has no preferential direction of spin-polarization (addressing different optical transitions may result in net polarization in either $m_s = 0$ or $m_s = \pm 1$), but should result in positive contrast

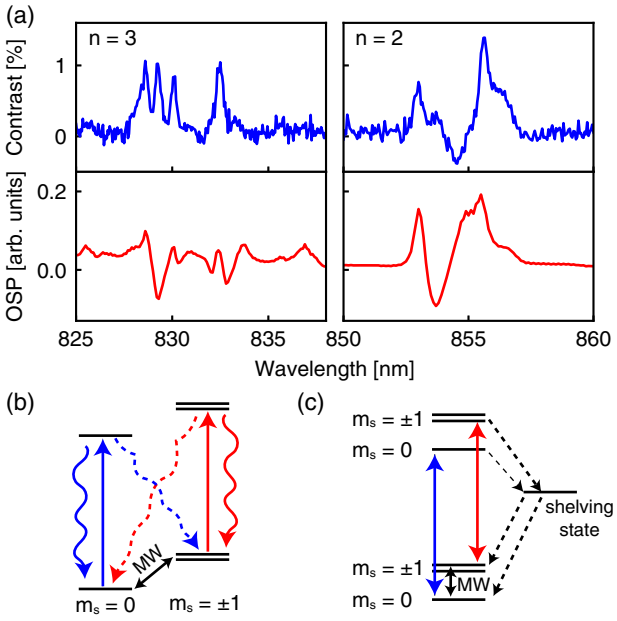

FIG. 4. Wavelength dependence of ODMR and mechanisms for ODMR contrast. (a) Upper panel: CW ODMR contrast as a function of excitation wavelength measured at 60 K. Microwave frequency is fixed at the lower hyperfine transition. Lower panel: OSP as a function of excitation wavelength at 5.5 K. ODMR contrast is measured at ambient magnetic field while OSP measurements are performed at X-band frequencies (~3100 G). (b) Level scheme for ODMR based on selective excitation of optical transitions with nonunity cyclicity. Dashed arrows indicate spin-non-conserving decay paths. (c) Level scheme for ODMR based on spin-dependent shelving. Dashed arrows represent nonradiative decay. Solid arrows indicate radiative transitions. MW denotes microwave driving.

(brighter emission) under resonant microwave driving, as population is restored to the state being addressed by the optical excitation.

Another possible mechanism involves spin-dependent shelving of population in the excited state into a metastable state, which then decays back to the ground state [Fig. 4(c)]. This mechanism is observed in the NV center under off-resonant excitation at room temperature. Here, the excitation addresses all spin sublevels in the ground state, and the different branching ratios in the excited state for different spin projections result in a spin polarization direction independent of excitation wavelength [53]. The sign of the ODMR contrast, however, has no such general restriction, and should depend on the specific details of the excited state manifold.

We compare the OSP and the ODMR contrast for the $n = 2$ and $n = 3$ BE transitions in Fig. 4(a). Spin polarization both *into* and *out of* the $m_s = 0$ state is observed, depending on the excitation wavelength. This suggests that optical pumping plays a role in the excitation cycle of these transitions. The ODMR contrast data, however, reveals that this is not a complete description. Although the $n = 3$ data

shows primarily positive contrast (brighter emission), the $n = 2$ data shows clear negative contrast for some excitation wavelengths. This suggests that decay from the excited state into a different manifold of states is involved.

In conclusion, we report the first realization of ODMR in SiV^0 centers in diamond. We demonstrate coherent control of an ensemble of SiV^0 spins at low magnetic field and measure T_1 much longer than 30 ms and T_2 of 55.5 μs at 6 K. ODMR is enabled by newly discovered higher-lying excited states of SiV^0, which allow for efficient optical spin polarization. We propose that these transitions arise from BE states, and we provide DFT calculations for the ionization threshold, central cell correction, and energy splitting between different states that are consistent with experimental observations. On-going work includes single center ODMR measurements, as well as investigating the microscopic mechanism for ODMR via BE states. Our measurements indicate that ODMR cannot arise solely from spin-dependent shelving of population or resonant optical pumping into a dark state, and it is likely that a combination of processes give rise to the observed features.

Optical spin polarization via these BE states enables a powerful method of spin initialization and readout for SiV^0 centers in diamond. In particular, their resonant nature allows for the use of much lower excitation powers, which circumvents optically induced noise from the bath [54]. More broadly, this scheme can potentially be deployed in other emerging defect systems, such as other neutral group IV vacancy centers in diamond [55,56] and neutral divacancy centers in SiC [57].

We thank J. Thompson for fruitful discussions, as well as S. Kolkowitz, L. Rodgers, and Z. Yuan for comments on the manuscript. This work was supported by the NSF under the EFRI ACQUIRE program (Grant No. 1640959) and through the Princeton Center for Complex Materials, a Materials Research Science and Engineering Center (Grant No. DMR-1420541). This material is also based on work supported by the Air Force Office of Scientific Research under Grant No. FA9550-17-0158, and was partly supported by DARPA under Grant No. D18AP00047. G. T. was supported by the János Bolyai Research Scholarship of the Hungarian Academy of Sciences and the ÚNKP-20-5 New National Excellence Program of the Ministry of Innovation and Technology in Hungary (ITM) from the National Research, Development and Innovation Office in Hungary (NKFIH). D. H. was supported by a National Science Scholarship from A*STAR, Singapore. A. G. acknowledges the support from NKFIH for Quantum Technology Program (Grant No. 2017-1.2.1-NKP-2017-00001) and National Excellence Program (Grant No. KKP129866), from the ITM and NKFIH for the Quantum Information National Laboratory in Hungary, from the EU Commission (Asteriqs project, Grant No. 820394) and the EU QuantERA program (Q_magine project, NKFIH Grant No. 127889).

*npdeleon@princeton.edu

[1] W. B. Gao, A. Imamoglu, H. Bernien, and R. Hanson, Nat. Photonics **9**, 363 (2015).
[2] M. Atatüre, D. Englund, N. Vamivakas, S.-Y. Lee, and J. Wrachtrup, Nat. Rev. Mater. **3**, 38 (2018).
[3] D. D. Awschalom, R. Hanson, J. Wrachtrup, and B. B. Zhou, Nat. Photonics **12**, 516 (2018).
[4] B. Hensen, H. Bernien, A. E. Drau, A. Reiserer, N. Kalb, M. S. Blok, J. Ruitenberg, R. F. L. Vermeulen, R. N. Schouten, C. Abelln, W. Amaya, V. Pruneri, M. W. Mitchell, M. Markham, D. J. Twitchen, D. Elkouss, S. Wehner, T. H. Taminiau, and R. Hanson, Nature (London) **526**, 682 (2015).
[5] J. Wolters, N. Sadzak, A. W. Schell, T. Schröder, and O. Benson, Phys. Rev. Lett. **110**, 027401 (2013).
[6] Y. Chu, N. P. de Leon, B. J. Shields, B. Hausmann, R. Evans, E. Togan, M. J. Burek, M. Markham, A. Stacey, A. S. Zibrov, A. Yacoby, D. J. Twitchen, M. Loncar, H. Park, P. Maletinsky, and M. D. Lukin, Nano Lett. **14**, 1982 (2014).
[7] P. E. Barclay, Kai-Mei C. Fu, C. Santori, A. Faraon, and R. G. Beausoleil, Phys. Rev. X **1**, 011007 (2011).
[8] B. C. Rose, D. Huang, Z.-H. Zhang, P. Stevenson, A. M. Tyryshkin, S. Sangtawesin, S. Srinivasan, L. Loudin, M. L. Markham, A. M. Edmonds, D. J. Twitchen, S. A. Lyon, and N. P. de Leon, Science **361**, 60 (2018).
[9] B. L. Green, M. W. Doherty, E. Nako, N. B. Manson, U. F. S. D'Haenens-Johansson, S. D. Williams, D. J. Twitchen, and M. E. Newton, Phys. Rev. B **99**, 161112(R) (2019).
[10] B. C. Rose, G. Thiering, A. M. Tyryshkin, A. M. Edmonds, M. L. Markham, A. Gali, S. A. Lyon, and N. P. de Leon, Phys. Rev. B **98**, 235140 (2018).
[11] A. M. Edmonds, M. E. Newton, P. M. Martineau, D. J. Twitchen, and S. D. Williams, Phys. Rev. B **77**, 245205 (2008).
[12] See Supplemental Material at http://link.aps.org/supplemental/10.1103/PhysRevLett.125.237402 for methods, additional characterization data, theoretical descriptions, and calculations, which includes Refs. [13–37].
[13] B. L. Green, S. Mottishaw, B. G. Breeze, A. M. Edmonds, U. F. S. D'Haenens-Johansson, M. W. Doherty, S. D. Williams, D. J. Twitchen, and M. E. Newton, Phys. Rev. Lett. **119**, 096402 (2017).
[14] A. Dietrich, K. D. Jahnke, J. M. Binder, T. Teraji, J. Isoya, L. J. Rogers, and F. Jelezko, New J. Phys. **16**, 113019 (2014).
[15] H.-P. Komsa, T. T. Rantala, and A. Pasquarello, Phys. Rev. B **86**, 045112 (2012).
[16] G. Makov and M. C. Payne, Phys. Rev. B **51**, 4014 (1995).
[17] C. Freysoldt, J. Neugebauer, and C. G. Van de Walle, Phys. Rev. Lett. **102**, 016402 (2009).
[18] S. Lany and A. Zunger, Phys. Rev. B **78**, 235104 (2008).
[19] W. Wu and A. J. Fisher, Phys. Rev. B **77**, 045201 (2008).
[20] J. M. Luttinger and W. Kohn, Phys. Rev. **97**, 869 (1955).
[21] C. Kittel and A. H. Mitchell, Phys. Rev. **96**, 1488 (1954).
[22] W. Kohn and J. M. Luttinger, Phys. Rev. **98**, 915 (1955).
[23] A. T. Collins, Phil. Trans. R. Soc. A **342**, 233 (1993).
[24] C. J. Rauch, in *Proceedings of the International Conference on the Physics of Semiconductors*, edited by A. C. Stickland (Institute of Physics and the Physical Society of London, 1962), pp. 276–280.

[25] F. Herman, C. D. Kuglin, K. F. Cuff, and R. L. Kortum, Phys. Rev. Lett. **11**, 541 (1963).
[26] J. Serrano, A. Wysmolek, T. Ruf, and M. Cardona, Physica (Amsterdam) **273B-274B**, 640 (1999).
[27] M. Willatzen, M. Cardona, and N. E. Christensen, Phys. Rev. B **50**, 18054 (1994).
[28] N. W. Ashcroft and N. D. Mermin, *Solid State Physics* (Holt, Rinehart and Winston, New York, 1976).
[29] A. Gali, E. Janzén, P. Deák, G. Kresse, and E. Kaxiras, Phys. Rev. Lett. **103**, 186404 (2009).
[30] E. Londero, G. Thiering, L. Razinkovas, A. Gali, and A. Alkauskas, Phys. Rev. B **98**, 035306 (2018).
[31] G. Kresse and J. Furthmüller, Phys. Rev. B **54**, 11169 (1996).
[32] S. Steiner, S. Khmelevskyi, M. Marsmann, and G. Kresse, Phys. Rev. B **93**, 224425 (2016).
[33] P. E. Blöchl, Phys. Rev. B **50**, 17953 (1994).
[34] O. Bengone, M. Alouani, P. Blöchl, and J. Hugel, Phys. Rev. B **62**, 16392 (2000).
[35] J. Heyd, G. E. Scuseria, and M. Ernzerhof, J. Chem. Phys. **118**, 8207 (2003).
[36] A. V. Krukau, O. A. Vydrov, A. F. Izmaylov, and G. E. Scuseria, J. Chem. Phys. **125**, 224106 (2006).
[37] J. P. Perdew, K. Burke, and M. Ernzerhof, Phys. Rev. Lett. **77**, 3865 (1996).
[38] A. M. Tyryshkin, S. Tojo, J. J. L. Morton, H. Riemann, N. V. Abrosimov, P. Becker, H.-J. Pohl, T. Schenkel, M. L. W. Thewalt, K. M. Itoh, and S. A. Lyon, Nat. Mater. **11**, 143 (2012).
[39] S. Felton, A. M. Edmonds, M. E. Newton, P. M. Martineau, D. Fisher, D. J. Twitchen, and J. M. Baker, Phys. Rev. B **79**, 075203 (2009).
[40] L. Allers and A. T. Collins, J. Appl. Phys. **77**, 3879 (1995).
[41] U. F. S. D'Haenens-Johansson, A. M. Edmonds, M. E. Newton, J. P. Goss, P. R. Briddon, J. M. Baker, P. M. Martineau, R. U. A. Khan, D. J. Twitchen, and S. D. Williams, Phys. Rev. B **82**, 155205 (2010).
[42] U. F. S. D'Haenens-Johansson, A. M. Edmonds, B. L. Green, M. E. Newton, G. Davies, P. M. Martineau, R. U. A. Khan, and D. J. Twitchen, Phys. Rev. B **84**, 245208 (2011).
[43] A. Gali and J. R. Maze, Phys. Rev. B **88**, 235205 (2013).
[44] T. Egilsson, J. P. Bergman, I. G. Ivanov, A. Henry, and E. Janzén, Phys. Rev. B **59**, 1956 (1999).
[45] L. Storasta, F. H. C. Carlsson, S. G. Sridhara, J. P. Bergman, A. Henry, T. Egilsson, A. Hallén, and E. Janzén, Appl. Phys. Lett. **78**, 46 (2001).
[46] J. Wagner, A. Dörnen, and R. Sauer, Phys. Rev. B **31**, 5561 (R) (1985).
[47] M. Kleverman, J.-O. Fornell, J. Olajos, H. G. Grimmeiss, and J. L. Lindström, Phys. Rev. B **37**, 10199 (1988).
[48] J. H. Svensson, B. Monemar, and E. Janzén, Phys. Rev. Lett. **65**, 1796 (1990).
[49] A. M. Frens, M. T. Bennebroek, A. Zakrzewski, J. Schmidt, W. M. Chen, E. Janzén, J. L. Lindström, and B. Monemar, Phys. Rev. Lett. **72**, 2939 (1994).
[50] N. T. Son, M. Singh, J. Dalfors, B. Monemar, and E. Janzén, Phys. Rev. B **49**, 17428 (1994).
[51] K. Pressel, A. Dörnen, G. Rückert, and K. Thonke, Phys. Rev. B **47**, 16267 (1993).
[52] M. Cardona and Y. Y. Peter, *Fundamentals of Semiconductors* (Springer, New York, 2005).
[53] L. Robledo, H. Bernien, T. van der Sar, and R. Hanson, New J. Phys. **13**, 025013 (2011).
[54] P. Siyushev, H. Pinto, M. Vörös, A. Gali, F. Jelezko, and J. Wrachtrup, Phys. Rev. Lett. **110**, 167402 (2013).
[55] G. Thiering and A. Gali, Phys. Rev. X **8**, 021063 (2018).
[56] G. Thiering and A. Gali, npj Comput. Mater. **5**, 18 (2019).
[57] W. F. Koehl, B. B. Buckley, F. J. Heremans, G. Calusine, and D. D. Awschalom, Nature (London) **479**, 84 (2011).